ACS APPLIED MATERIALS & INTERFACES

Research Article

www.acsami.org

Large-Scale Assembly of Organic Micro/Nanocrystals into Highly Ordered Patterns and Their Applications for Strain Sensors

Chao Gong,† Wei Deng,† Bin Zou, Yuliang Xing, Xiujuan Zhang,* Xiaohong Zhang,* and Jiansheng Jie*

Institute of Functional Nano & Soft Materials (FUNSOM) & Collaborative Innovation Center of Suzhou Nano Science and Technology, Jiangsu Key Laboratory for Carbon-Based Functional Materials & Devices, Soochow University, Suzhou, Jiangsu 215123, P. R. China

Supporting Information

ABSTRACT: Large-scale assembly of zero-dimensional (0-D) organic nano/microcrystals into desired patterns is essential to their applications. However, current methods can hardly apply to the 0D organic crystals because of their relatively large sizes and polyhedral structures. Here, we demonstrate a facile and convenient way to assemble organic single crystals into large-area two-dimensional (2D) structures by application of appropriate electric field (EF). The ordering of the 2D structure depends on the frequency and field strength of the external electric field. Furthermore, lithographically patterning electrodes offer an efficient way to assemble the crystals into controllable patterns. By tuning the electrode pattern geometry, various desirable patterns with variable microstructures can be achieved. These formed superstructures and patterns can be fixed on the electrodes through exerting an external direct current, which allows for the further utilization of the patterns. With assistance of adhesive tape, patterns could be transferred onto flexible substrates for constructing a highly sensitive strain sensor. This strategy is applicable to nonsphere organic crystals with different sizes to assemble at desired positions and construct highly ordered arrays in a large scale, which opens new possibilities of organic microcrystals application in new-generation electronic devices and sensors.

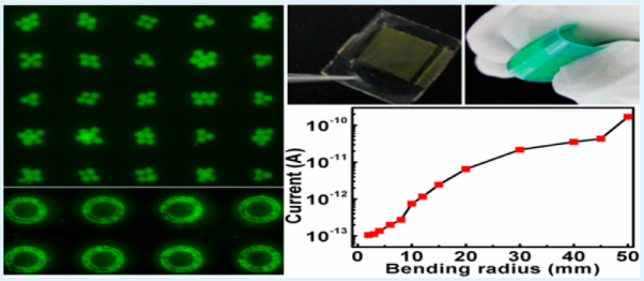

KEYWORDS: *organic micro/nanocrystals, 2,5,8,11-tetra-tert-butylperylene (TBPe), electric field, electrohydrodynamic (EHD) flows, assembly, strain sensors*

INTRODUCTION

Organic semiconductors have attracted increasing interest due to their strikingly different electronic and optical properties from their inorganic counterparts.[1−3] Organic single crystals are promising candidates for application in low-cost microelectronics and optoelectronics[4−6] because they offer better carrier transport properties and superior performance compared with the corresponding thin films, which are attributed to their lack of grain boundaries and molecular disorder. Some unique applications have been successfully achieved from organic micro/nanocrystals, such as organic photovoltaics,[7−9] optical waveguides and lasers,[10−13] and field-effect transistors,[14−17] which demonstrate great potential as building blocks for the next generation of miniaturized electronic and optoelectronic devices. However, to extend the practical applications of organic micro/nanocrystals in integrated devices and complex circuits, large-scale assembly and patterning of the nanocrystals with high order at desired positions must be achieved.[18−22] Arrangement of the crystals into highly ordered patterns reduces the occurrence of parasitic current paths (i.e., cross-talk) between neighboring devices and results in significant decrease in "off" current.[23] Most electronic applications also require good alignment and precise patterning of nanostructures with high controllability to achieve the expected performance.

To assemble the organic micro/nanocrystals, two major strategies have been developed over the past decades. One is, in vapor phase, through managing the roughness of the substrate to control the nucleation sites, which made it possible for selective growth of organic crystals in designated locations.[24−28] The other is, in solution phase, through alternatively modulating the surface wettability of the substrate, so that molecules can selectively form nuclei at hydrophilic areas and continue their further growth into crystals, leaving behind desirable patterns.[29−33] Template-assisted evaporation can also induce the selective growth of organic crystals for patterning.[34−36] In these strategies, assembly and patterning are achieved by the selective growth of crystals at designated positions. However, in most cases, high-quality organic micro/nanocrystals are usually needed to grow in certain conditions that are not generally appropriate for simultaneously patterning.[37,38] Therefore, most high-quality organic micro/nanocrystals are produced with random orientations and the

Received: September 4, 2013
Accepted: June 23, 2014
Published: July 2, 2014

methods discussed above are not effective for their patterning. It is also noted that these methods are mainly suitable for the patterned growth of one-dimensional (1D) organic micro/nanowires and two-dimensional (2D) nanosheets, while the patterned growth/assembly of zero-dimensional (0D) organic micro/nanocrystals is not demonstrated yet. This is likely due to the relatively large sizes (size >1 μm) and polyhedral structures of the 0D organic micro/nanocrystals. As such, determination of a general approach for the large-scale assembly of randomly dispersed 0D organic crystals into desired patterns and construction of highly ordered arrays is a significant endeavor that can help promote the practical applications of organic micro/nanocrystals.

Herein, we demonstrate a new strategy to assemble randomly dispersed organic crystals into large-area 2D compact monolayers with desired patterns by applying an appropriate electric field (EF) in an indium tin oxide (ITO) glass cell.[39] Various patterns can be selectively produced on exposed ITO areas by manipulating the electrode geometries through photolithography. The patterns obtained could be readily transferred onto flexible and insulative substrates via a feasible stamp method for further device application. Notably, the whole process could be accomplished in a time-efficient manner; only 1−2 min were sufficient to achieve ordered assembly of the 0-D organic crystals. To demonstrate the effectiveness of this strategy in practical applications, we constructed a strain sensor based on the patterned organic micro/nanocrystals, which demonstrated excellent strain-sensing properties with outstanding device stability and repeatability. Furthermore, the method is applicable to the large-scale assembly of other randomly dispersed organic crystals, thus extending their potential in diverse fields such as integrated devices and photonic crystals.

EXPERIMENTAL DETAILS

In a typical synthesis of TBPe crystals, 1 mL of 1 mmol L^{-1} TBPe/THF solution was injected into 5 mL of 8.3 g/L Pluronic 123 in water at room temperature. After 5 min of stirring, the sample was left to stand for stabilization. As-prepared TBPe crystals were cleaned with deionized water several times to remove residual surfactant.[40] To synthesize DCM particles, we injected 400 μL of 2 mmol L^{-1} DCM/THF solution into 5 mL of deionized water. After 5 min of stirring, the sample was left undisturbed for another 4 h. Sonication was then applied to the sample for 10 min.

Photolithography was used to prepattern the bottom ITO electrode surface with a photoresist (PR) layer. The bottom ITO substrate was cleaned with acetone and ethanol, ultrasonicated for 15 min, and then treated with UV (ultraviolet) rays-ozone for 15 min. The PR was spin-coated onto the ITO substrate at thickness of ~1 μm and then selectively exposed to UV rays. After development and washing with water, the prepatterned ITO was formed. The experimental setup consisted of two parallel pieces of conductive ITO glass (2 cm × 2 cm) separated by thick double-sided tape (90 to 100 μm). The crystals were dispersed in deionized water, subjected to 10 min of ultrasonication, and then injected into the cell. A function generator (Caltek CA1645) was used to generate an EF between the ITO electrodes. The applied voltage ranged from 0 to 20 V and the *f* ranged from 0 to 5 MHz. A digital imaging camera (Leica DFC 420C) mounted on a Leica DM4000 M optical microscope was used to monitor the assembly process. A direct current supply (SAKO SK1761SL2A) was applied between the ITO electrodes for 2 s with a voltage of 12 V to fix crystal patterns to the bottom ITO electrode after the desired structure was obtained. SEM images were obtained using a scanning electron microscope (Quanta 200 FEG). *I*−*V* characteristics of the TBPe patterns were measured using a semiconductor characterization system (Keithley 4200-SCS).

RESULTS AND DISCUSSION

Polyhedral microcrystals of 2,5,8,11-tetra-tert-butylperylene (TBPe) with different sizes were prepared by a previously reported surfactant-assisted self-assembly method.[40] Their size distributions are shown in Figure S1 in the Supporting Information. The microcrystals have sizes of 0.6 ± 0.3 μm, 1.4 ± 0.8 μm, and 2.5 ± 1.2 μm, respectively. To assess the electrical characteristics of the TBPe microcrystals, they were first dispersed in water and then drop-casted onto prepatterned Au source-drain electrodes on SiO_2/Si substrate (see Figure S2 in the Supporting Information). When gate voltage was applied on the Si substrate, the device exhibited pronounced gating effect with current on/off ratio >10^4. The mobility of the TBPe microcrystals could be estimated to be 3.2 × 10^{-4} $cm^2/(V\ s)$. This value is comparable to previous report on TBPe film (7 × $10^{-5}$$cm^2/(V\ s)$).[41] The relatively high mobility makes the TBPe microcrystals an promising system for the applications in electronic devices.

The aqueous suspension of TBPe microcrystals was sandwiched in a glass cell composed of two pieces of conductive ITO glass (see Figure S3 in the Supporting Inforamtion). These microcrystals were first dispersed randomly in the cell undergoing Brownian motion in water. When an EF was applied normally to the two ITO glass electrodes, the crystals quickly moved to the surface of the electrodes and began to aggregate into homogeneous nuclei at the bottom of the cell. Particles around these nuclei gradually

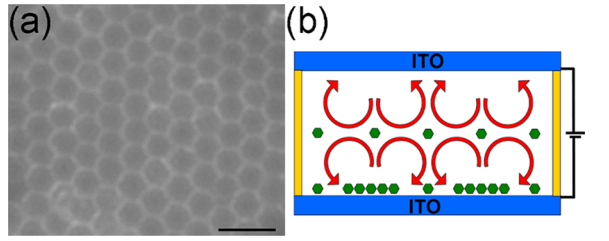

Figure 1. (a) Dark field optical microscopy image of 2D structure formed with rhombic dodecahedral TBPe crystals. Scale bar is 10 μm. (b) Schematic illustration of electrohydrodynamic flow (red arrowheads) in the ITO glass cell.

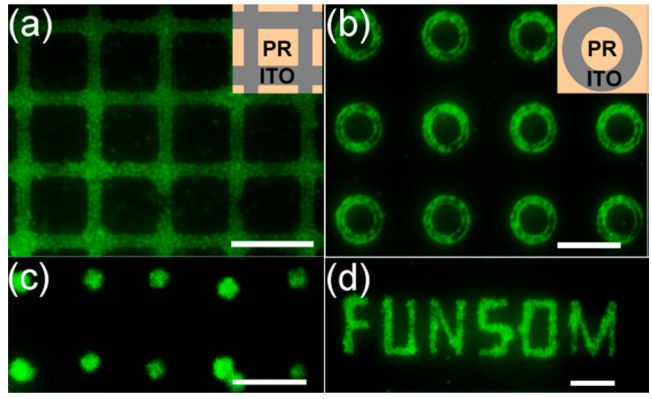

Figure 2. Fluorescence microscopy images of the patterns formed on the ITO substrate with different photoresist patterns: (a) gridlike structure, (b) concentric circles, (c) single-particle arrangement, and (d) a label of "FUNSOM". Insets in a and b show schematic illustrations of the corresponding PR patterns on the ITO substrate. Scale bars are (a, d) 20 μm for, (b) 50 μm, and (c) 10 μm.

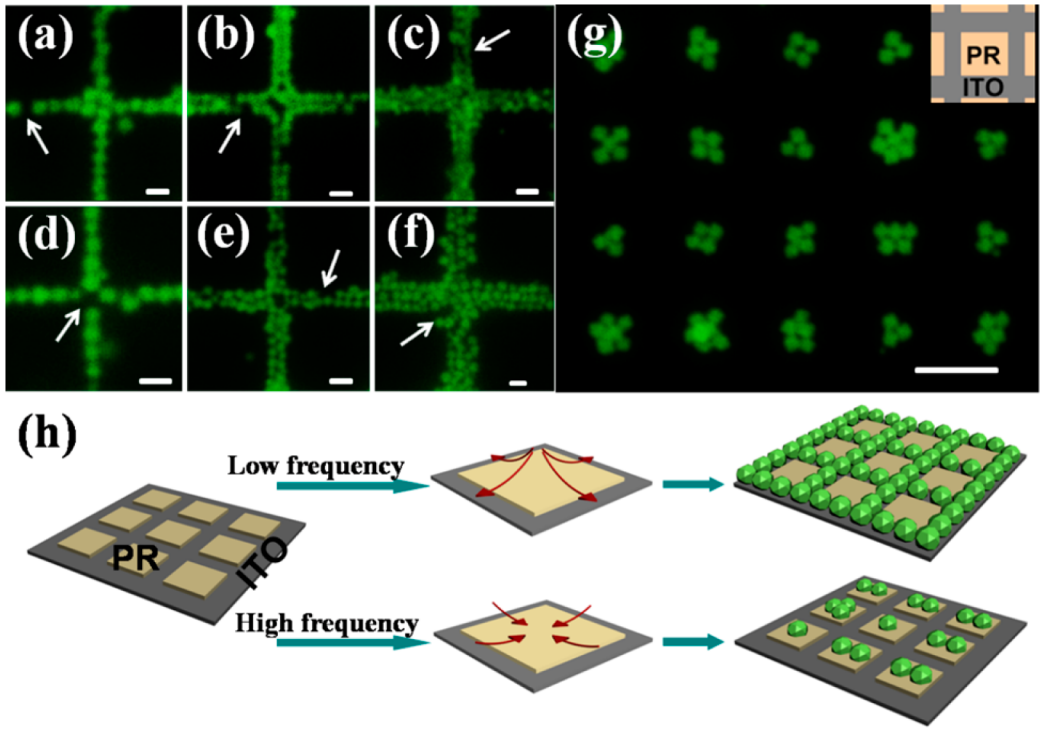

Figure 3. Fluorescence microscopy images of crossed patterns with particles of (a) 2.5 μm, (b) 1.4 μm, and (c) 600 nm patterned on the same gridlike substrate (3 μm in width). Fluorescence microscopy images of crossed patterns with the same TBPe particle (2 μm in diameter) on a grid-like substrate with channels of (d) 2, (e) 4, and (f) 6 μm. (g) A fluorescence microscopy image of a pattern formed on a grid-like patterned substrate under $E = 10 \times 10^4$ V/m and $f = 30000$ Hz. Scale bars are (a–f) 5 and (g) 20 μm. (h) Schematic illustrations of the assembly directions (red arrowheads) of TBPe crystals under low and high frequencies on patterned ITO substrates.

moved toward the nuclei and accumulated (see Figure S4 in the Supporting Information). Assembly was ceased when all of the particles in the bulk solution had been transported onto the ITO surface, leaving behind ordered 2D structures. This process could be accomplished in a short time of 1–2 min. From Figure 1a, it is seen that the 2D assemblies are highly oriented, hexagonally close-packed. The regularity of the 2D structures varied reversibly with the EF turned on/off. When the EF was turned off, particles began to move in a random way and the structure became disordered (see Figure S5b in the Supporting Information), whereas the particles would get together again and assembled into ordered structures within several seconds with the EF applied again (see Figure S5c in the Supporting Information). This process was repeatable, which gives strong evidence that EF acts as the main driving force for the aggregation and assembly of the crystals. The strength (E) and frequency (f) of the EF were also found to play key roles in the formation of the ordered structures. When the f was tuned from 100 Hz to 5 MHz at a fixed $E = 4.5 \times 10^4$ V/m, ordered 2-D structures were only formed at a certain f window (100–1200 Hz, see Figure S7a–c in the Supporting Information). Beyond this window, particles tended to be disordered. The effect of E was also examined at a fixed $f = 500$ Hz. Particles were packed tightly at relatively high $E = 3.2 \times 10^4$ V/m and became loose as E gradually decreased to 2.7×10^4 V/m. At $E = 2.2 \times 10^4$ V/m, a disordered structure was obtained (see Figure S5d–f in the Supporting Information). We have also performed a statistical measurement of interparticle distance under different f at a fixed $E = 4.0 \times 10^4$ V/m and under different E at a fixed $f = 500$ Hz (see Figure S6 in the Supporting Information). It is seen that the interparticle distance increases with increasing frequency from 400 to 2000 Hz, whereas it decreases with increasing the field strength from 1.2×10^4 to 4.5×10^4 V/m.

When an EF is applied normally to the two ITO glass electrodes, the presence of particles in the cell can cause spatial perturbations in the lateral current distribution, resulting in induction of electrohydrodynamic (EHD) flows (Figure 1b) that can transfer the particles to the bottom surface of the electrode.[42] The nature of the EHD flows is believed to be the main attractive force behind the 2D colloidal assembly under an EF, whereas dipole–dipole interactions between adjacent particles are the main repulsive force. At low f and fixed E, the EHD interaction is the main attractive interaction to assemble particles together. However, with the f getting higher (>1000 Hz), this interaction decreases and tends to be repulsive, which makes the structure incompact.[43,44] If f is fixed, the field strength affects both the EHD interaction and dipole–dipole interaction in the same way. The decrease of the field strength makes the interaction among the particles become smaller, and then the interparticle space becomes larger, until the interaction is too low to prevail against Brownian motion.[44]

Inspired by the above results, we introduced a photolithography patterning technique into the assembly process, which allowed further precise control over the crystal assembly. The bottom ITO electrode was first prepatterned as a grid using PR layer by photolithography. Upon application of an EF, particles can selectively transfer to the exposed ITO areas and form patterns under appropriate E (>4.0×10^4 V/m) and f (<1000 Hz). Combined with photolithography patterning technique, pattern shapes could be varied with the lithographic bottom pattern geometries. Images a and b in Figure 2 show that gridlike and concentric circular patterns were successfully

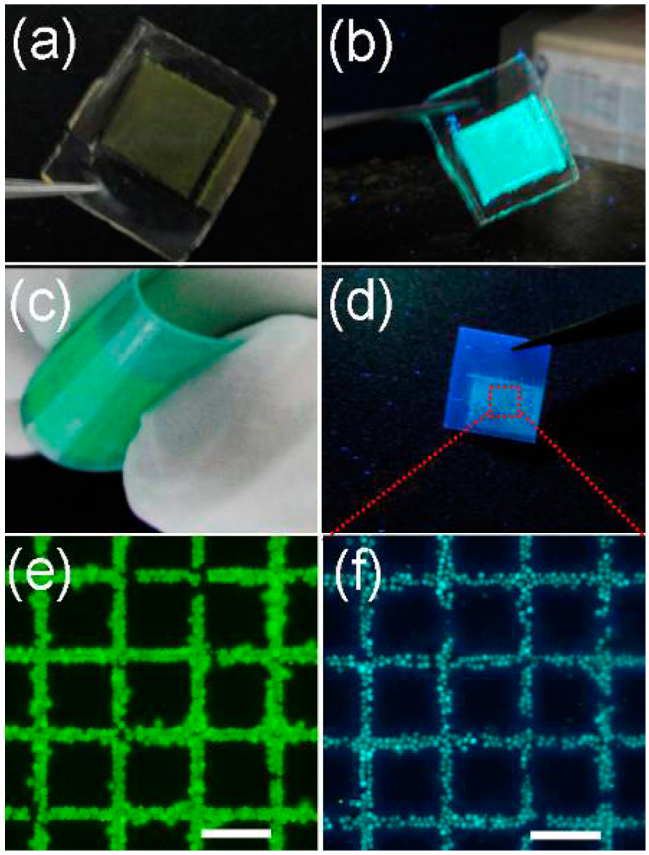

Figure 4. Optical images of as-prepared TBPe nanoparticle patterns on ITO substrate under (a) ambient light and (b) irradiation with an ultraviolet (UV) lamp of 365 nm. Optical images of the patterns transferred onto a mechanically flexible tape under (c) ambient light and (d) UV irradiation, respectively. Fluorescence microscopy images of the patterns on (e) the ITO substrate and (f) flexible tape. Scale bars are 20 μm.

fabricated on the bottom electrodes. Patterns of individual particles or complex structures may also be readily obtained. A single-particle arrangement can be achieved using a patterned substrate with a discrete opening ITO area of about 2 μm in diameter. Figure 2c shows that most opening area is filled with one particle with a diameter of about 2 μm; the yield for the single particle patterning could be as high as 90%. Patterns with a desired complex label (FUNSOM) are also easily formed, as shown in Figure 2d.

Microstructures of the patterned assemblies can be precisely tuned by controlling either the particle size or the exposed ITO area. For example, the width of the exposed ITO channel could be fixed at 3 μm by photolithography patterning, crossed patterns with individual, double and several particle lines could be formed with particles in size of 2.5, 1.4, and 0.6 μm, respectively (Figure 3a–c). Similar results could also be achieved by changing the width of the exposed ITO channels. As shown in Figure 3d–f, patterns with individual, double, and several particle (2 μm in diameter) lines may be formed in ITO channel widths of 2, 4, and 6 μm, respectively. Although defects are frequently observed in the assembled patterns, as indicated by the arrows in Figure 3a–f, this preliminary result still reveals the great potential of manipulating and positioning the organic microcrystals with unprecedented accuracy with the aid of an electric field.

It should be noted that when f was increased over 10000 Hz, particles inversely left the ITO bands and transferred to PR areas, forming separated islands at the center of the squares (Figure 3g). This result indicates that pattern shapes are not determined by the exposed ITO geometries at high f (see Figure S8a, c in the Supporting Information) but by the shape of the center of the PR (see Figure S8b, d in the Supporting Information). Moreover, by varying the particle concentration in the solution, the number of particles gathered on the PR square centers could be tuned from few to many (see Figure S9 in the Supporting Information).

As illustrated in Figure 3h, the presence of PR layers on a conductive ITO substrate could generate current inhomogeneities on the surface of the electrode at low f (<1000 Hz). The current gradient could induce long-range EHD flows along the electrode toward higher-current-density areas.[45] These EHD flows could carry particles to the ITO regions.[46,47] Once the particles accumulate at the ITO regions, localized EHD flows are generated, further carrying the particles closer to each other and assembling into the ordered structures as described on the flat ITO surface.[48] However, we note that a minimum frequency of 100 Hz is needed to achieve the effect patterning of particles on ITO regions (see Figure S10 in the Supporting Information). At high f (>10 000 Hz), the size and intensity of long-range EHD flows decreases, which lowered their ability to transfer particles toward ITO regions.[46,47] Localized EHD interactions also tend to be repulsive under high f,[43,44] causing particles to repel each other at ITO regions. The decreased long-range EHD flows and the repulsive localized EHD interactions among the particles cause particle movement from ITO regions to PR areas. Because of the symmetrical geometry of the ITO areas around the PR squares, these particles would finally find their equilibrium positions at the centers of the PR squares.

The desired patterns can be achieved over large areas using the proposed strategy, which is of great importance in practical device applications. Patterns of organic crystals can be spread over almost the entire lithographic ITO substrate, as shown in Figure 4a. Unfortunately, the fact that the patterns formed on ITO areas need to be maintained with an EF could greatly restrict their application. To address this problem, a direct current was exerted between the ITO electrodes to induce a strong attractive electrostatic force between particles and at the bottom ITO electrode to fix the micro/nanostructures firmly to the substrate. After the EF was withdrawn and the substrate was treated with washing and drying processes, the patterns can still be well preserved, as shown in Figure S11 in the Supporting Information. This strategy of EF-induced patterning can be extended to other organic crystals. Figure S12 in the Supporting Information shows the parallel patterning of 4-(dicyanomethylene)-2-methyl-6-(4-dimethylaminostyryl)-4H-pyran nanoparticles, which clearly demonstrated the generalizability of this method. On the other hand, we found that temperature also plays an important role in manipulation process (see Figure S13 in the Supporting Information); lower temperature is beneficial to the formation of ordered structure with best result achieving at room temperature. This can be attributed to the more drastic Brownian motion at higher temperature.

Transfer of the resulting patterns from the ITO to an insulative substrate allows utilization of the micro/nanocrystals in practical applications. In this study, an thermal release tape (3M, thickness ~0.15 mm) was used as an elastic stamp to achieve the transfer.[49] Simply by attaching the tape on the

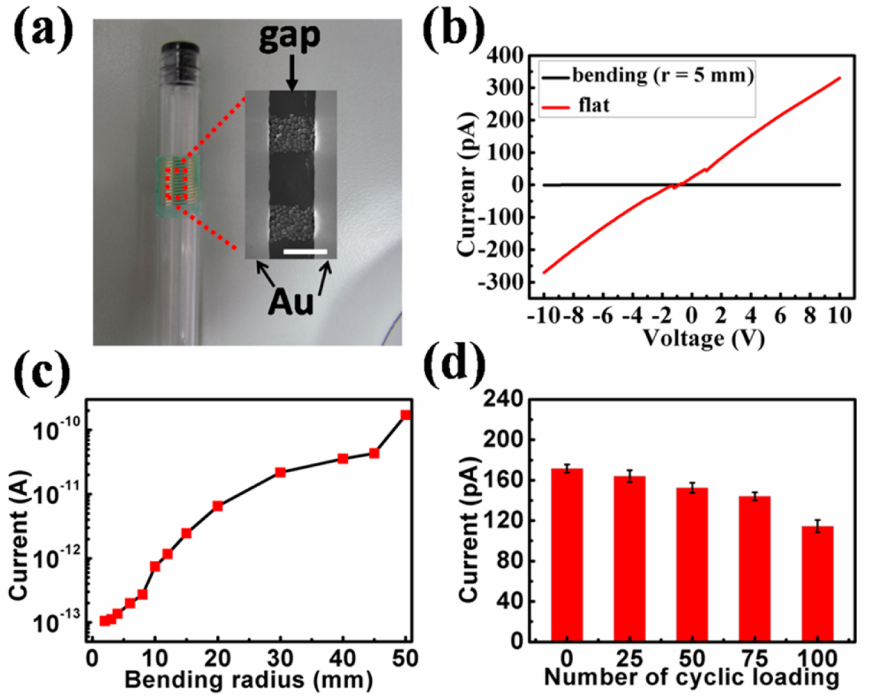

Figure 5. (a) Photograph of the flexible device rolled on a columned pen. Inset shows the SEM image of a typical device. Scale bar is 10 μm. (b) $I-V$ curves of the device before (red curve) and after bending (black curve). (c) Device current as a function of bending radius. (d) Device current as a function of bending cycles. The current was measured when the device was flat at each cycle.

patterns and then peeling it off, particle patterns could be perfectly transferred from ITO (Figure 4a, b) onto the mechanically flexible stamp (Figure 4c, d), whereas the photoresist patterns will retain on the ITO substrate (see Figure S14 in the Supporting Information). Fluorescence microscopy images in Figure 4e, f show that the morphologies and structures of the patterns remained intact after the transfer, making the next device fabrication possible..

It is known that the organic materials are largely incompatible with conventional photolithography technique, though the latter has been widely used in current microelectronic industry. To overcome this difficulty, in this work, we develop a simple transfer printing method to achieve the large-scale fabrication of devices based on the patterned TBPe microcyrstals. In this method, the microcrystal patterns were first transferred to flexible tape, and then the tape, along with the microcrystal patterns on it, was pressed against on a Si substrate with predefined Au electrode pairs (interspace 10 μm). Next, the tape was slowly peeled off from the Si substrate. Because of the higher adhesiveness of the tape, the Au electrodes would be released from the substrate and adhered to the tape, resulting in the formation of top-contact devices based on the TBPe microcyrstals (see Figures S15 and S16 in the Supporting Information, and Figure 5a). Figure 5b shows the $I-V$ measurements performed on the device. The device exhibited good Ohmic contact with a typical current of about 1×10^{-10} A when flat. By contrast, the current decreased dramatically when the device was bent to a bending radius (r) of 5 mm by rolling around a columnar device as shown in Figure 5a. Figure 5c further plots the relation of current as a function of bending radius from 2 to 50 mm. It is noted that the current decreases with the decrease of bending radius, reaching values almost identical to that obtained from the blank electrode when r = 2 mm (1×10^{-13} A). The decrease in current may be attributed to disruption of the contact between neighboring particles upon bending. Figure 5d shows the change of the device current during repeated bending cycles at the same radius of 5 mm. All of the current data were collected in the flat state. The device exhibited good stability, with the current remaining ~70% of original value even after 100 circles of bending and relaxation. These results suggest that as-prepared devices based on patterned organic particles have promising potential as strain sensors. Normally, the device can operate in air for about 1 week, but further prolonging the time leads to the obvious degradation of device performance. The instability of the organic microcrystals in air and the part dissolution of the microcrystals in the glue on the flexible tape may be responsible for this result. On the other hand, we also observed the decrease of device current with the increase of detecting temperature (see Figure S17 in the Supporting Information). This is likely caused by the enhanced dissolution of organic microcrystals into the glue. Another possible reason is the thermal expansion and deformation of the substrate (tape). Nevertheless, it is expected that the device lifetime could be remarkably improved if appropriate encapsulation methods as well as other more suitable substrates are used. Besides strain sensor, the granular structure of this device is also suitable for gas sensor. We have performed a preliminary investigation on the sensor performance of the device by blowing the device with N_2 gas, as shown in Figure S18 in the Supporting Information. It is seen that the current decreases dramatically when the N_2 gas is turn on, while the current gradually recovers to the original value after switching off the gas. This can be attributed to the desorption of water molecules from the nanocrystals under the blowing of the N_2 gas.

CONCLUSION

In summary, we have developed a convenient method to rapidly assemble randomly dispersed organic crystals into large-

area 2D monolayers with desired patterns using an external EF. Attractive and repulsive interactions among the particles can be well controlled by changing either the E or f to modulate the interparticle distance and order of assembly. Appropriate design of electrode geometries by lithography techniques, can make organic crystals selectively patterning on the exposed conductive area, producing various patterns with shapes from grid-like structure and concentric circles to any designed complex labels. Particularly, it is found that particles not only assemble on exposed ITO areas at low f (<1000 Hz) but also form assemblies at the center of PR areas at high f (>10 000 Hz). Patterns can be transferred onto flexible substrates for practical application in devices. A strain sensor fabricated with the patterns described above showed excellent performance with good repeatability even after one hundred circles of bending and relaxation. The proposed method is applicable to various organic crystals for controlled patterning, which would facilitate their applications in integrated devices and complex circuits. It also opens up the opportunities for designing and fabricating novel photonic devices, such as photonic crystals, based on the 0D organic micro/nanocrystals because of their comparable sizes with the light wavelength.

■ ASSOCIATED CONTENT

Ⓢ Supporting Information

SEM images and the particle-size distribution of the TBPe polyhedral microcrystals. FET characteristics of the TBPe particles. Sketch of the experimental setup. Dark-field optical microscopy images of TBPe rhombic dodecahedral particles at different assembly stages. Dark-field optical microscope images of the order to disorder phase transition of the assembled structure. Particle distance as a function of frequency and field strength. Dark-field optical microscope images of the assemble structure formed under different conditions. Optical microscope images of the patterns formed at different EF frequency. Fluorescence microscope images of the patterns formed at the center of the photoresist squares at high EF frequency. Optical microscope images of the TBPe polyhedral microcrystal patterns formed under different f. The fixed patterns formed on the ITO substrate after applying a DC field shortly (2 s) on the electrodes. Fluorescence microscopy images of patterns consisted of 4-(Dicyanomethylene)-2-methyl-6-(4-dimethylaminostyryl)-4H-pyran DCM particles. Fluorescence microscope images of the TBPe polyhedral microcrystal patterns formed at different temperature. Schematic illustration of the device fabrication process. Optical images show the transfer process of electrode patterns. The change of device current with temperature. Current response of the device with N_2 on/off under a voltage bias of +10 V. This material is available free of charge via the Internet at http://pubs.acs.org.

■ AUTHOR INFORMATION

Corresponding Authors

*E-mail: jsjie@suda.edu.cn. Tel: +86-512-65881265.
*E-mail: xjzhang@suda.edu.cn. Tel: +86-512-65880955.
*E-mail: xhzhang@mail.ipc.ac.cn. Tel: +86-10-82543510.

Author Contributions

†C.G. and W.D. contributed equally to this work. The manuscript was written through contributions of all authors. All authors have given approval to the final version of the manuscript.

Notes

The authors declare no competing financial interest.

■ ACKNOWLEDGMENTS

This work was supported by National Basic Research Program of China (973 Program, Grants 2013CB933500, 2012CB932400), Major Research Plan of the National Natural Science Foundation of China (Grants 91027021, 91233110), National Natural Science Foundation of China (Grants 51173124, 51172151), the Natural Science Foundation of Jiangsu Province (BK20131162), and a Project Funded by the Priority Academic Program Development of Jiangsu Higher Education.

■ REFERENCES

(1) Li, R. J.; Hu, W. P.; Liu, Y. Q.; Zhu, D. B. Micro- and Nanocrystals of Organic Semiconductors. *Acc. Chem. Res.* **2010**, *43*, 529−540.

(2) Coropceanu, V.; Cornil, J.; da Silva, F. D. A.; Olivier, Y.; Silbey, R.; Bredas, J. Charge Transport in Organic Semiconductors. *Chem. Rev.* **2007**, *107*, 926−952.

(3) Zang, L.; Che, Y.; Moore, J. S. One-Dimensional Self-Assembly of Planar π-Conjugated Molecules: Adaptable Building Blocks for Organic Nanodevices. *Acc. Chem. Res.* **2008**, *41*, 1596−1608.

(4) Shirota, Y. Organic Materials for Electronic and Optoelectronic Devices. *J. Mater. Chem.* **2000**, *10*, 1−25.

(5) Kwon, J. E.; Park, S. Y. Advanced Organic Optoelectronic Materials: Harnessing Excited-State Intramolecular Proton Transfer (ESIPT) Process. *Adv. Mater.* **2011**, *23*, 3615−3642.

(6) Zhang, X. J.; Jie, J. S.; Zhang, W.; Zhang, C.; Luo, L.; He, Z.; Zhang, X. H.; Zhang, W. J.; Lee, C. S.; Lee, S. T. Photoconductivity of a Single Small-Molecule Organic Nanowire. *Adv. Mater.* **2008**, *20*, 2427−2432.

(7) Yoon, S. M.; Lou, S. J.; Loser, S.; Smith, J.; Chen, L. X.; Facchetti, A.; Marks, T. Fluorinated Copper Phthalocyanine Nanowires for Enhancing Interfacial Electron Transport in Organic Solar Cells. *Nano Lett.* **2012**, *12*, 6315−6321.

(8) Chang, C. Y.; Wu, C. E.; Chen, S. Y.; Cui, C.; Cheng, Y. J.; Hsu, C. S.; Wang, Y. L.; Li, Y. Enhanced Performance and Stability of a Polymer Solar Cell by Incorporation of Vertically Aligned, Cross-Linked Fullerene Nanorods. *Angew. Chem., Int. Ed.* **2011**, *50*, 9386−9390.

(9) Yang, F.; Shtein, M.; Forrest, S. R. Morphology Control and Material Mixing by High-Temperature Organic Vapor Phase Deposition and Its Application to Thin-Film Solar Cells. *J. Appl. Phys.* **2005**, *98*, 014906−014906−10.

(10) Zhao, Y. S.; Zhan, P.; Kim, J.; Sun, C.; Huang, J. Patterned Growth of Vertically Aligned Organic Nanowire Waveguide Arrays. *ACS Nano* **2010**, *4*, 1630−1636.

(11) Koos, C.; Vorreau, P.; Vallaitis, T. All-Optical High-Speed Signal Processing with Silicon-Organic Hybrid Slot Waveguides. *Nat. Photonics* **2009**, *3*, 216−219.

(12) Balzer, F.; Bordo, V. G.; Simonsen, A. C. Optical Wave Guiding in Individual Nanometer-Scale Organic Fibers. *Phys. Rev. B* **2003**, *67*, 115408.

(13) Kozlov, V. G.; Parthasarathy, G.; Burrows, P. E. Structures for Organic Diode Lasers and Optical Properties of Organic Semiconductors Under Intense Optical and Electrical Excitations. *IEEE J. Quantum Electron.* **2000**, *36*, 18−26.

(14) Tang, Q.; Li, H.; Song, Y.; Xu, W.; Hu, W.; Jiang, L.; Liu, Y.; Wang, X.; Zhu, D. B. In Situ Patterning of Organic Single-Crystalline Nanoribbons on a SiO_2 Surface for the Fabrication of Various Architectures and High-Quality Transistors. *Adv. Mater.* **2006**, *18*, 3010−3014.

(15) Facchetti, A. Semiconductors for Organic Transistors. *Mater. Today* **2007**, *10*, 28−37.

(16) Dimitrakopoulos, C. D.; Malenfant, P. R. L. Organic Thin Film Transistors for Large Area Electronics. *Adv. Mater.* **2002**, *14*, 99−117.
(17) Mcculloch, L.; Ashraf, R. S.; Biniek, L. Design of Semiconducting Indacenodithiophene Polymers for High Performance Transistors and Solar Cells. *Acc. Chem. Res.* **2012**, *45*, 714−722.
(18) Zhang, Y. P.; Wang, X.; Wu, Y.; Jie, J.; Zhang, X.; Xing, Y.; Wu, H.; Zou, B.; Zhang, X.; Zhang, X. Aligned Ultralong Nanowire Arrays and Their Application in Flexible Photodetector Devices. *J. Mater. Chem.* **2012**, *22*, 14357−14362.
(19) Briseno, A. L.; Roberts, M.; Ling, M.; Moon, H.; Nemanick, E. J.; Bao, Z. N. Patterning Organic Semiconductors Using "Dry" Poly(dimethylsiloxane) Elastomeric Stamps for Thin Film Transistors. *J. Am. Chem. Soc.* **2006**, *128*, 3880−3881.
(20) Acharya, S.; Hill, J. P.; Ariga, K. Soft Langmuir−Blodgett Technique for Hard Nanomaterials. *Adv. Mater.* **2009**, *21*, 2959−2981.
(21) Long, Y. Z.; Yu, M.; Sun, B.; Gu, C. Z.; Fan, Z. Recent Advances in Large-Scale Assembly of Semiconducting in Organic Nanowires and Nanofibers for Electronics, Sensors and Photovoltaics. *Chem. Soc. Rev.* **2012**, *41*, 4560−4580.
(22) Jin, Y.; Yang, D.; Kang, D.; Jiang, X. Fabrication of Necklace-Like Structures via Electrospinning. *Langmuir* **2010**, *26*, 1186−1190.
(23) Liu, S. H.; Wang, W. M.; Briseno, A. L.; Mannsfeld, S. C.; Bao, Z. N. Controlled Deposition of Crystalline Organic Semiconductors for Field-Effect-Transistor Applications. *Adv. Mater.* **2009**, *21*, 1217−1232.
(24) Briseno, A. L.; Mannsfeld, S. C.; Ling, M. M.; Liu, S.; Tseng, R. J.; Reese, C.; Roberts, M.; Yang, Y.; Wudl, F.; Bao, Z. N. Patterning Organic Single-Crystal Transistor Arrays. *Nature.* **2006**, *444*, 913−917.
(25) Liu, S. H.; Mannsfeld, S. C. B.; Wang, W. M.; Sun, Y.; Stoltenberg, R. M.; Bao, Z. N. Patterning of α-Sexithiophene Single Crystals with Precisely Controlled Sizes and Shapes. *Chem. Mater.* **2008**, *21*, 15−17.
(26) Wang, W.; Zhong, D.; Zhu, J.; Kalischewski, F.; Dou, R.; Wedeking, K.; Wang, Y.; Heuer, A.; Fuchs, H.; Erker, G.; Chi, L. F. Patterned Nucleation Control in Vacuum Deposition of Organic Molecules. *Phys. Rev. Lett.* **2007**, *98*, 225504.
(27) Wang, W.; Du, C.; Bi, H.; Sun, Y.; Wang, Y.; Mauser, C.; Como, E. D.; Fuchs, H.; Chi, L. F. Tunable Multicolor Ordered Patterns with Two Dye Molecules. *Adv. Mater.* **2010**, *22*, 2764−2769.
(28) Mbenkum, B. N.; Barrena, E.; Zhang, X. N.; Kelsch, M.; Dosch, H. Selective Growth of Organic 1-D Structures on Au Nanoparticle Arrays. *Nano Lett.* **2006**, *6*, 2852−2855.
(29) Tong, Y. H.; Tang, Q.; Lemke, H. T.; Poulsen, K. M.; Westerlund, F.; Hammershøj, P.; Bechgaard, K.; Hu, W.; Bjørnholm, T. Solution-Based Fabrication of Single-Crystalline Arrays of Organic Nanowires. *Langmuir* **2010**, *26*, 1130−1136.
(30) Briseno, A. L.; Aizenberg, J.; Han, Y.; Penkala, R. A.; Moon, H.; Lovinger, A. J.; Kloc, C.; Bao, Z. N. Patterned Growth of Large Oriented Organic Semiconductor Single Crystals on Self-Assembled Monolayer Templates. *J. Am. Chem. Soc.* **2005**, *127*, 12164−12165.
(31) Minari, T.; Liu, C.; Kano, M.; Tsukagoshi, K. Controlled Self-Assembly of Organic Semiconductors for Solution-Based Fabrication of Organic Field-Effect Transistors. *Adv. Mater.* **2012**, *24*, 299−306.
(32) Liu, N. L.; Zhou, Y.; Wang, L.; Peng, J.; Wang, J.; Pei, J.; Cao, Y. In Situ Growing and Patterning of Aligned Organic Nanowire Arrays via Dip Coating. *Langmuir* **2008**, *25*, 665−671.
(33) Mannsfeld, S. C. B.; Sharei, A.; Liu, S.; Roberts, M. E.; McCulloch, I.; Heeney, M.; Bao, Z. N. Highly Efficient Patterning of Organic Single-Crystal Transistors from the Solution Phase. *Adv. Mater.* **2008**, *20*, 4044−4048.
(34) Bao, R. R.; Zhang, C.; Wang, Z.; Zhang, X.; Ou, X.; Lee, C. S.; Jie, J. S.; Zhang, X. H. Large-Scale Controllable Patterning Growth of Aligned Organic Nanowires through Evaporation-Induced Self-Assembly. *Chem.—Eur. J.* **2012**, *18*, 975−980.
(35) Li, H. Y.; Tee, B. C. K.; Cha, J. J.; Cui, Y.; Chung, J. W.; Lee, S. Y.; Bao, Z. N. High-Mobility Field-Effect Transistors from Large-Area Solution-Grown Aligned C_{60} Single Crystals. *J. Am. Chem. Soc.* **2012**, *134*, 2760−2765.
(36) Li, H. Y.; Tee, B. C. K.; Giri, G.; Chung, J. W.; Lee, S. Y.; Bao, Z. N. High-Performance Transistors and Complementary Inverters Based on Solution-Grown Aligned Organic Single-Crystals. *Adv. Mater.* **2012**, *24*, 2588−2591.
(37) Zhang, X. J.; Zhang, X.; Wang, B.; Zhang, C.; Chang, J. C.; Lee, C. S.; Lee, S. T. One- or Semi-Two-Dimensional Organic Nanocrystals Induced by Directional Supramolecular Interactions. *J. Phys. Chem. C* **2008**, *112*, 16264−16268.
(38) Qiu, Y. F.; Chen, P.; Liu, M. Evolution of Various Porphyrin Nanostructures via an Oil/ Aqueous Medium: Controlled Self-Assembly, Further Organization, and Supramolecular Chirality. *J. Am. Chem. Soc.* **2010**, *132*, 9644−9652.
(39) Sullivan, M. T.; Zhao, K.; Hollingsworth, A. D.; Austin, R. H.; Russel, W. B.; Chaikin, P. M. An Electric Bottle for Colloids. *Phys. Rev. Lett.* **2006**, *96*, 015703.
(40) Zhang, X. J.; Dong, C.; Zapien, J. A.; Ismathullakhan, S.; Kang, Z.; Jie, J. S.; Zhang, X.; Chang, J. C.; Lee, C. S.; Lee, S. T. Polyhedral Organic Microcrystals: From Cubes to Rhombic Dodecahedra. *Angew. Chem., Int. Ed.* **2009**, *48*, 9121−9123.
(41) Wu, C. C.; Hung, Y. W. Carrier Transport Properties in TBPe Measured by Time-of-Flight System. *Bull. Coll. Eng., Natl. Taiwan Univ.* **2003**, *88*, 61−66.
(42) Yeh, S. R.; Seul, M.; Shraiman, B. I. Assembly of Ordered Colloidal Aggregrates by Electric-Field-Induced Fluid Flow. *Nature* **1997**, *386*, 57−59.
(43) Ristenpart, W. D.; Aksay, I. A.; Saville, D. A. Assembly of Colloidal Aggregates by Electrohydrodynamic Flow: Kinetic Experiments and Scaling Analysis. *Phys. Rev. E* **2003**, *69*, 021405.
(44) Zhang, K. Q.; Liu, X. Y. Two Scenarios for Colloidal Phase Transitions. *Phys. Rev. Lett.* **2006**, *96*, 105701.
(45) Ristenpart, W. D.; Jiang, P.; Slowik, M. A.; Punckt, C.; Saville, D. A.; Aksay, I. A. Electrohydrodynamic Flow and Colloidal Patterning near Inhomogeneities on Electrodes. *Langmuir* **2008**, *24*, 12172−12180.
(46) Bhatt, K. H.; Grego, S.; Velev, O. D. An AC Electrokinetic Technique for Collection and Concentration of Particles and Cells on Patterned Electrodes. *Langmuir* **2005**, *21*, 6603−6612.
(47) Nadal, F.; Argoul, F.; Kestener, P.; Pouligny, B.; Ybert, C.; Ajdari, A. Electrically Induced Flows in the Vicinity of a Dielectric Stripe on a Conducting Plane. *Eur. Phys. J. E* **2002**, *9*, 387−399.
(48) Xie, R. G.; Liu, X. Y. Electrically Directed On-Chip Reversible Patterning of Two-Dimensional Tunable Colloidal Structures. *Adv. Funct. Mater.* **2008**, *18*, 802−809.
(49) Lee, C. H.; Kim, D. R.; Zheng, X. L. Fabricating Nanowire Devices on Diverse Substrates by Simple Transfer-Printing Methods. *Proc. Natl. Acad. Sci. U.S.A.* **2010**, *107*, 9950−9955.